Photorefractive Index Modulation in Chiral Smectic Phases

Roberto Termine and Attilio Golemme*

Dipartimento di Chimica, Università della Calabria, 87036 Rende, Italy

Received: September 18, 2001; In Final Form: January 25, 2002

We have developed a model to calculate the refractive index modulation in photorefractive chiral smectic A and C materials. The index pattern is calculated considering the simultaneous presence of a sinusoidal space-charge field and an applied field. The material parameters considered by the model are the principal indices of refraction of the mesophase, the relative amplitude of the applied and space-charge field, the electroclinic coefficient (for S_A*), and the spontaneous tilt angle (for S_C*). The model also takes into account the sample orientation and light polarization. Results show large variations of the index modulation with the various paremeters considered. Experimental data obtained from polymer-dispersed chiral smectic A samples are in excellent agreement with the predictions of the model.

I. Introduction

In recent years, a variety of materials for applications in the field of optical data processing and storage have been developed. Such applications are based on several different physical properties, and among these, photorefractivity is one of the most interesting and promising. The photorefractive effect[1,2] is based on the photogeneration of mobile charges under nonuniform illumination: the charges redistribute in space by diffusion and eventually by field-induced drift, generating a space-charge electric field. If the refractive index of the material is field-dependent, the net effect is a phase-shifted refractive index replica of the initial illumination pattern. There are several other different phenomena (photoisomerization, photoinduced chemical reactions, etc.) that can be exploited to modulate the refractive index using light, but only in photorefractive materials are the refractive index and the light patterns phase-shifted. This fact has very interesting consequences, including the possibility of energy exchange between the different light beams that generate a photorefractive index grating.

Although the first photorefractive materials were inorganic crystalline salts,[3] the search for easily processable, inexpensive, and chemically flexible substances led researchers toward the development of organic media with photorefractive properties,[4,5] and among these, polymers have proven to be extremely interesting.[6,7] Although in crystalline salts the conduction of photogenerated electrons and holes can be understood in terms of the energy bands' structure, in solid amorphous organics, it is usually described using activated hopping models.[8] The field dependence of the refractive index was instead at first attributed to the nonlinear optical properties of chromophores, often pendants in a side-chain polymer or dissolved molecules. In fact, it was soon realized[9] that the nonlinear optical response alone could not be responsible for the high index modulations that were observed and that contributions due to the birefringence induced by the high electric fields used to pole the chromophores had to be taken into account.

This led the way to the development of liquid crystalline photorefractive materials in which birefringence is high and spontaneous, thus eliminating the problems associated with the use of intense poling fields. The first photorefractive mesophases were nematics doped with photosensitive substances.[10−12] In this case, the space-charge field setup is due to diffusion of photogenerated ions, although competition with hole hopping has been reported.[13] In addition, highly efficient photorefractive materials have been obtained using dispersions of nematic domains in photoconducting polymers.[14,15] In this case, the space-charge field is generated as usual in the polymer matrix, and the refractive index modulation is due to the field-induced reorientation of the nematic director in the microdomains. More recently, reports of smectic mesophases with photorefractive properties have appeared[16−18] where the director reorientation is not, as in nematics, a quadratic effect in the field due to dielectric anisotropy. In the case of ferroelectric chiral smectic C (S_C*) phases, the field-induced director reorientation is associated with the reorientation of the spontaneous polarization,[19] but in chiral smectic A (S_A*) phases, it is due to an induced polarization through the so-called linear electroclinic effect.[20] The driving forces behind the development of such smectic photorefractive materials are their possible bistability and their fast reorientation times, which can be as low as 10 μs instead of the 1−10 ms typical of most nematic devices, although in photorefractive applications such short times have not yet been reported.

To optimize the photorefractive performance of smectic materials, it is necessary to understand how the index modulation depends on a variety of parameters. In this work, we present a simple model to calculate the refractive index modulation associated with the director reorientation in photorefractive S_A* and S_C* phases. The model takes into account several material parameters as well as the direction and the polarization of the incident beams. In section II, we will describe the calculation of the local director orientation in S_A* phases under the simultaneous influence of an applied and a photogenerated electric field, and in section III, we will complete the task of obtaining the refractive index modulation by also taking into account the polarization and direction of the incident light and the orientation of the smectic layers. A comparison with experimental data will also be given in this section. In section IV, we will extend the calculations to the S_C* phases, and in

* Corresponding author. E-mail: a.golemme@unical.it. Fax: +39 0984 492044.

10.1021/jp013567q CCC: $22.00
Published on Web 04/03/2002

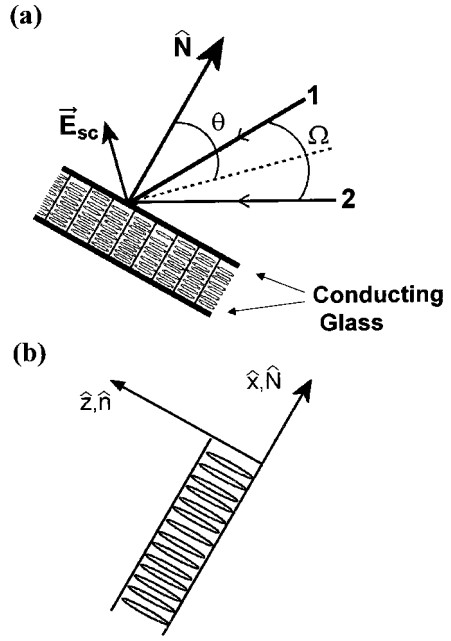

Figure 1. (a) Illustration of sample orientation with respect to the two writing beams. Light beams are indicated with 1 and 2, and the other symbols are defined in the text. Smectic layers dimensions are not to scale. (b) Enlargement of one of the smectic layers.

section V, we will summarize our results. Finally, in section VI, we will describe the details of the experimental setup and the sample preparation.

II. Director Orientation in S_A* Phases

In our model, we will assume the presence of a sinusoidal space-charge field generated in a photoconducting medium by two overlapping coherent beams. The description of the details of the setup of such a field and of its phase shift relative to the interference pattern lies outside of the aim of our article. In addition, in the calculation of the director orientation, we will include only the effect of the electric fields and will neglect the contributions of elastic energy, which means that we assume that field-induced distortions are small or distributed over long distances.

Let us consider two "writing" beams overlapping on a uniformly aligned sample of a substance in the S_A* phase, as illustrated in Figure 1. The sample normal $\hat{N}$ and the two writing beams are in the same plane, the *p* plane, and in the absence of fields, the smectic director $\hat{n}$ is homogeneously aligned along the layer normal $\hat{z}$, which is also normal to $\hat{N}$, as illustrated in Figure 1a, where the plane of the Figure is the *p* plane. The angle between the two writing beams is Ω, and the angle between the beams bisector and the sample normal is θ. In Figure 1b, which is an enlargment of one of the layers of Figure 1a, we define a reference system with $\hat{n}$ along $\hat{N}$, $\hat{z}$ along the layer normal, and $\hat{y}$ as in a right-handed system. In general, we can orient our sample in such a way that $\hat{z}$ is not in the *p* plane but at an angle defined by δ in Figure 2. It is useful to define a new reference system independent from sample rotation, with versors $\hat{x}_0$ coincident with $\hat{x}$ and $\hat{N}$, $\hat{z}_0 = \hat{z}(\delta = 0)$ fixed in the *p* plane, and $\hat{y}_0 = \hat{y}(\delta = 0)$ so that $(\hat{x}, \hat{y}, \hat{z})$ and $(\hat{x}_0, \hat{y}_0, \hat{z}_0)$ are identical for $\delta = 0$.

Because of the electroclinic effect,[21] illustrated in Figure 3, in S_A* phases, an electric field $\vec{E}$ in the plane of the layers will induce a director rotation around the field itself by an angle $\alpha = e_c E$. The sign of the electroclinic coefficient e_c indicates a

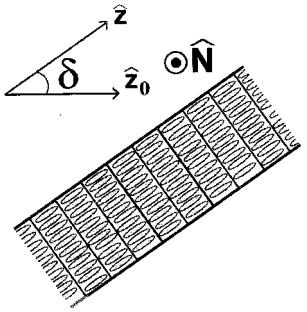

Figure 2. Different view of sample orientation. In this case, the *p* plane containing the writing beams, $\hat{z}_0$ and $\hat{N}$, is normal to the plane of the Figure. Both conducting glasses that border the sample are parallel to the plane of the Figure.

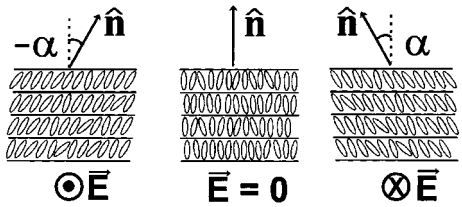

Figure 3. Illustration of the electroclinic effect in S_A* phases.

clockwise or counterclockwise rotation. In our case, the total electric field is the sum of two contributions: an applied field $\vec{E}_0$ directed along $\hat{x}$ and a space-charge field $\vec{E}_{SC}$ obtained using the interference of two coherent light beams overlapping on the sample through the photogeneration of mobile charges. The applied field is necessary in organic photorefractive media to increase the photogeneration efficiency and to provide a charge-drift mechanism. With the geometrical arrangement described in Figure 1, $\vec{E}_{SC}$ will always lie in the *p* plane, and assuming a sinusoidal form, it can be described as

$$\vec{E}_{SC} = E_{SC} \cos \frac{2\pi\xi}{\Lambda} \hat{\xi} \qquad (1)$$

where Λ is the grating spacing and the versor $\hat{\xi}$ is in the $(\hat{x}_0, \hat{z}_0)$ plane, with components depending on θ. We assume that in our materials E_{SC} is proportional to the component of the applied field in the grating direction (i.e., $E_{SC} = kE_0 \sin \theta$ with $k \leq 1$). This assumption may not be valid for all applied fields and it is not essential for our calculations, but in the following discussion we will consider it so that we may simplify our results and focus the attention of the reader on the main implications of the model.

In addition, although $\vec{E}_0$ is always directed within the smectic layers, $\vec{E}_{SC}$ can have a component along the layer normal $\hat{z}$. Given the negative dielectric anisotropy of the S_A* phase, the effect of this component will be to increase to some extent the director rotation due to the electroclinic effect induced by the field components within the smectic layer. This corresponds to an effective increase of the electroclinic coefficient, and because the $\hat{z}$ component of $\vec{E}_{SC}$ vanishes for $\delta = \pm \pi/2$, such an increase will be larger as δ approaches 0 or π. The total effect can be viewed as an increase of the background refractive index with a negligible influence on the index modulation. For this reason, in the following discussion we will neglect the $\vec{E}_{SC}$ component in the direction of the layer normal.

The calculation of director orientation is straightforward for $\delta = 0$. In this case, the components of E_{SC} in the $(\hat{x}, \hat{y}, \hat{z},)$ frame will be $(E_{SC} \sin \theta, 0, E_{SC} \cos \theta)$, with E_{SC} defined in eq 1, and the total field in the plane of the layers $\vec{E}_{TL}$ will be directed along $\hat{x}$:

$$\vec{E}_{TL} = \left[\pm E_0 + E_{SC} \sin\theta \cos\frac{2\pi\xi}{\Lambda}\right]\hat{x} = E_0\left[\pm 1 + k \sin^2\theta \cos\frac{2\pi\xi}{\Lambda}\right]\hat{x} \quad (2)$$

The ± sign depends on the direction of $\vec{E}_0$. The director will then be rotated around $\hat{x}$ by an angle

$$\alpha = e_c E_{TL} = e_c E_0\left[\pm 1 + k \sin^2\theta \cos\frac{2\pi\xi}{\Lambda}\right] \quad (3)$$

where α is the angle between the local director $\hat{n}$ and $\hat{z}$. As an example, for $\vec{E}_0$ along $+\hat{x}$ and a positive e_c, as we move along ξ, the angle α will oscillate between a maximum and a minimum value defined by

$$\alpha = e_c E_0[1 \pm k \sin^2\theta] \quad (4)$$

as described in Figure 4.

For $\delta \neq 0$, the calculation of director orientation is not as simple. Let us first find the components of the space-charge field amplitude in the $(\hat{x}, \hat{y}, \hat{z})$ frame. As illustrated in Figure 5, the direction of $\vec{E}_{SC}$ can be defined by the angle φ between $\vec{E}_{SC}$ and $\hat{z}$ and the angle γ between $\vec{E}_{SC}$ and $\hat{y}$, which are both functions of δ. The angle between $\vec{E}_{SC}$ and $\hat{x}$ is constant at $\pi/2 - \theta$. We have

$$\cos\varphi = \cos\theta \cos\delta \quad (5a)$$

$$\cos\gamma = \cos\theta \cos(\pi/2 - \delta) = \cos\theta \sin\delta \quad (5b)$$

and for the space-charge field components, we have

$$E_{SCx} = kE_0 \sin^2\theta \cos 2\pi\xi/\Lambda \quad (6a)$$

$$E_{SCy} = kE_0 \sin\theta \cos\theta \sin\delta \cos 2\pi\xi/\Lambda \quad (6b)$$

$$E_{SCz} = kE_0 \sin\theta \cos\theta \cos\delta \cos 2\pi\xi/\Lambda \quad (6c)$$

The component of $\vec{E}_{SC}$ normal to the layers is E_{SCz}. We can easily obtain the total field amplitude in the plane of the layers, which is due to E_0, E_{SCx} and E_{SCy}:

$$E_{TL} = E_0\left[\left(\pm 1 + k \sin^2\theta \cos\frac{2\pi\xi}{\Lambda}\right)^2 + k^2 \sin^2\theta \cos^2\theta \sin^2\delta \cos^2\frac{2\pi\xi}{\Lambda}\right]^{1/2} \quad (7)$$

The direction of $\vec{E}_{TL}$ can be defined by the angle β between $\vec{E}_{TL}$ and $\hat{x}$ given by

$$\tan\beta_{\pm} = \frac{k \sin\theta \cos\theta \sin\delta \cos\frac{2\pi\xi}{\Lambda}}{\pm 1 + k \sin^2\theta \cos\frac{2\pi\xi}{\Lambda}} \quad (8)$$

where the $\beta_{\pm}$ angles correspond to the choice of $\vec{E}_0$ directed along $+\hat{x}$ or $-\hat{x}$.

As a consequence of the electroclinic effect, the field $\vec{E}_{TL}$ will induce a rotation of the director by an angle

$$\psi_A = e_c E_{TL} = e_c E_0\left[\left(\pm 1 + k \sin^2\theta \cos\frac{2\pi\xi}{\Lambda}\right)^2 + \left(k \sin\theta \cos\theta \sin\delta \cos\frac{2\pi\xi}{\Lambda}\right)^2\right]^{1/2} \quad (9)$$

where a positive or negative sign of ψ_A, depending on the sign of the electroclinic coefficient e_c, indicates a right-handed or left-handed rotation around $\vec{E}_{TL}$, respectively. Knowing β and ψ_A, as illustrated in Figure 6, we can now easily find the components of the director:

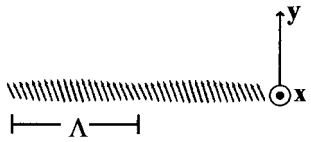

Figure 4. Variation of director orientation, defined by α, along the grating wavevector direction for $\delta = 0$. The y component is enlarged 20 times for clarity. Data for α were obtained from eq 3 for $k = 0.7$, $e_c = 0.19$ deg μm/V, $\theta = 31°$, and $E_0 = 40$ V/μm.

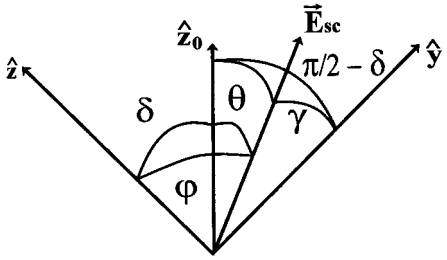

Figure 5. Schematic illustration of the angles defining the orientation of $\vec{E}_{SC}$ for $\delta \neq 0$. The versors $\hat{y}$, $\hat{z}$, and $\hat{z}_0$ are always within the same plane.

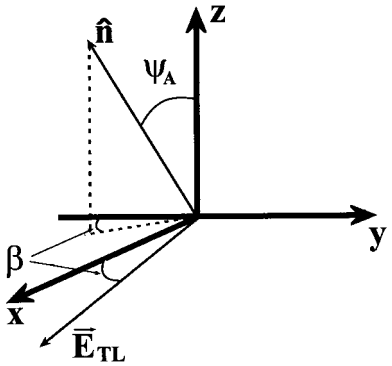

Figure 6. Illustration of the director tilt due to the electroclinic effect. The (x, y) plane is the plane of the smectic layers.

$$n_x = \sin\psi_A \sin\beta \quad (10a)$$

$$n_y = -\sin\psi_A \cos\beta \quad (10b)$$

$$n_z = \cos\psi_A \quad (10c)$$

In Figure 7, we show for the case $\delta = 45°$ the projections of the director on the yz and xy (the smectic layer) planes as a function of ξ. It is evident that for the reasonable material parameters used in the calculation, the space-charge field-induced rotation of the director is not very large, although, as discussed in the following section, it may correspond to a refractive index modulation ranging between 10^{-3} and 10^{-2} in the case of bulk samples (note that for clarity in Figure 7 the scales of the different components of the director are different).

III. Refractive Index Modulation in S_A* Phases

In photorefractive smectic materials, the refractive index modulation will strongly depend on the polarization of light. Considering beam 1 of Figure 1, we can define its polarization using a versor $\hat{e}$, and we can introduce a versor $\hat{p}$ in the p plane that is normal to the incoming beam and has a positive $\hat{z}_0$ component. The angle η between $\hat{e}$ and $\hat{p}$ will define the polarization direction, and $0 \leq \eta \leq \pi$. With the aim of obtaining

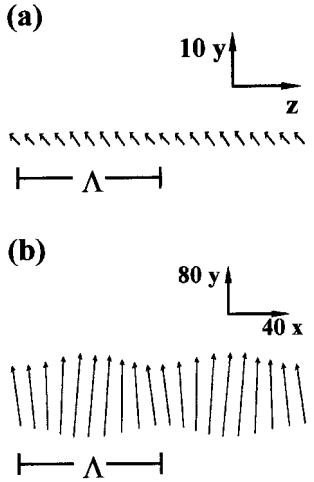

Figure 7. Variation of the director orientation along the grating wavevector direction for $\delta \neq 0$, obtained using eqs 8−10. In (a), we show the *y* and *z* components of the director, and the *y* component is enlarged 10 times for clarity. In (b), the *x* (enlarged 40 times) and *y* (enlarged 80 times) components are shown. Data were obtained using $k = 0.7$, $e_c = 0.19$ deg μm/V, $E_0 = 40$ V/μm, $\theta = 31°$, and $\delta = 45°$.

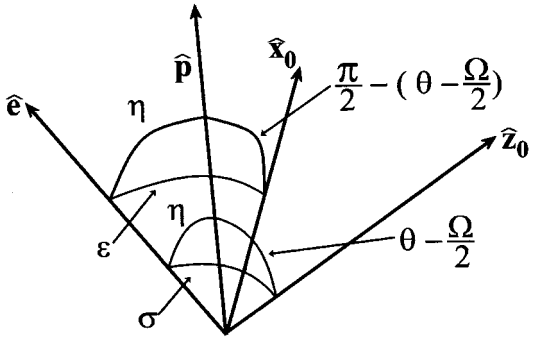

Figure 8. Schematic illustration of the orientation of the polarization versor $\hat{e}$.

the components of $\hat{e}$ in the $(\hat{x}, \hat{y}, \hat{z})$ frame, we will first find them in the $(\hat{x}_0, \hat{y}_0, \hat{z}_0)$ frame. Considering Figure 8, we have

$$e_{x_0} = \cos\epsilon = \cos\eta\cos\left[\frac{\pi}{2} - \left(\theta - \frac{\Omega}{2}\right)\right] = \cos\eta\sin\left(\theta - \frac{\Omega}{2}\right) \tag{11a}$$

$$e_{y_0} = \cos\left(\frac{\pi}{2} + \eta\right) = -\sin\eta \tag{11b}$$

$$e_{z_0} = \cos\sigma = \cos\eta\cos\left(\theta - \frac{\Omega}{2}\right) \tag{11c}$$

We can obtain the $(\hat{x}, \hat{y}, \hat{z})$ frame from the $(\hat{x}_0, \hat{y}_0, \hat{z}_0)$ frame by rotating the last one by an angle δ around $\hat{x}_0$. It is then easy to obtain the components of $\hat{e}$ in the $(\hat{x}, \hat{y}, \hat{z})$ frame starting from eq 11 as

$$e_x = e_{x_0} = \cos\eta\sin\left(\theta - \frac{\Omega}{2}\right) \tag{12a}$$

$$e_y = -\sin\eta\cos\delta + \cos\eta\sin\delta\cos\left(\theta - \frac{\Omega}{2}\right) \tag{12b}$$

$$e_z = \sin\eta\sin\delta + \cos\eta\cos\delta\cos\left(\theta - \frac{\Omega}{2}\right) \tag{12c}$$

For beam 2, we obtain similar equations where the term $(\theta - \Omega/2)$ is replaced by $(\theta + \Omega/2)$.

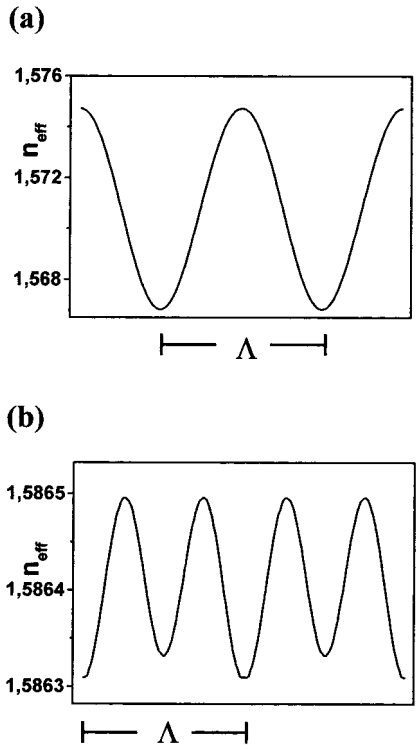

Figure 9. Refractive index modulation along the grating wavevector calculated from eq 13 for (a) $k = 0.7$, $e_c = 0.19$ deg μm/V, $E_0 = 40$ V/μm, $n_o = 1.5$, $n_e = 1.6$, $\theta = 31°$, $\Omega = 1°$, $\delta = 60°$, and $\eta = 30°$ and (b) the same parameters as were used in (a) but with $\eta = 66.8°$.

The effective refractve index can now be obtained:

$$n_{\text{eff}} = \frac{n_o n_e}{\sqrt{n_e^2\sin^2\Phi + n_o^2\cos^2\Phi}} \tag{13}$$

n_o and n_e are the ordinary and extraordinary refractive indices of the liquid crystal, respectively, and Φ is the angle between $\hat{e}$ and the director $\hat{n}$ that is obtained from eqs 10 and 12 as

$$\cos\Phi = e_x n_x + e_y n_y + e_z n_z \tag{14}$$

Using eq 13, we can obtain the effective refractive index, which is modulated along the direction defined by the grating wavevector as described in Figure 9a for given values of the various parameters, as indicated in the caption. It is interesting that for certain relative values of polarization and sample orientation a component of the grating develops with a wavevector that is twice the wavevector of the space-charge field, as illustrated in Figure 9b, even if in our model we consider a single harmonic space-charge field. This happens when $|\delta - \eta|$ is smaller than an angle on the order of ψ_A, and it is a consequence of the oscillations of the director on both sides of the polarization direction as the space-charge field changes sign. For $|\delta - \eta|$ within this range, the grating component at the fundamental of the space-charge field is greatly reduced, and the diffraction efficiency should drop substantially.

As previously described, the index modulation depends on different material (k, e_c, n_o, n_e) and geometrical (θ, Ω, δ, η) parameters. The dependence on material parameters is straightforward, with the modulation increasing for larger k, e_c, and $n_e - n_o$ values. The k parameter describes the relative magnitudes of the space-charge and applied fields, which is of paramount importance in determining the efficiency of photorefractive liquid crystals[22] and of any material in which birefringence

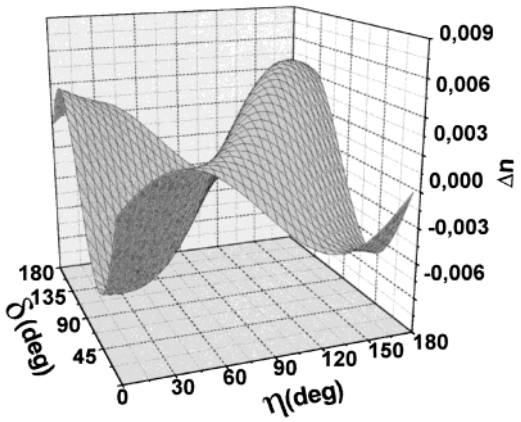

Figure 10. Refractive index modulation Δn in a S_A* phase as a function of δ and η, calculated from eq 13 for $k = 0.7$, $e_c = 0.19$ deg μm/V, $E_0 = 40$ V/μm, $n_o = 1.5$, $n_e = 1.6$, $\theta = 31°$, and $\Omega = 1°$.

contributions to the index modulation are important. The mesophase index variation for a given field is determined instead by the induced tilt (controlled by the electroclinic coefficient e_c) and by the birefringence $n_e - n_o$. Variation of the grating amplitude with the angles θ and Ω is to be expected, but it should mainly be a consequence of the variation of the space-charge field intensity because the grating spacing and the component of the applied field in the grating direction would be affected. For this reason, this dependence is outside the scope of this article. Instead, it is extremely useful to consider the effect on the gratings of δ and η, which is illustrated in Figure 10 for a set of realistic values of the other parameters. In this Figure, we show, as obtained using eq 13, the δ and η dependence of Δn, which is the difference in the refractive indices calculated at the points where the space-charge field is maximized and minimized (i.e., $\Delta n = n(E_{SCmax}) - n(E_{SCmin})$). As previously mentioned, for certain values of δ and η, this Δn component vanishes even if the modulation is still present at higher Fourier components (see Figure 9b).

From Figure 10, it is also evident that the sign of Δn can be positive or negative for different values of δ and η, corresponding to different directions of energy exchange in two-beam coupling experiments. In particular, given a certain sample orientation (δ), the sign of the gain coefficient can be changed by changing the polarization of light. In addition, for a given δ, there will be a certain polarization (η) for which the index modulation is at a maximum. In Figure 11, we show the value of $|\Delta n|$ as a function of δ and η obtained using the same values of the parameters as were used in Figure 10. With the parameters we used for the computation, we have two nearly equivalent maxima for ($\delta \approx 75°$, $\eta \approx 30°$) and for ($\delta \approx 110°$, $\eta \approx 140°$). As Figure 11 clearly shows, a careful relative choice of δ and η is necessary to maximize index modulation.

To evaluate the correctness of our model, we performed measurements of the first-order diffraction efficiency as a function of η in stretched polymer-dispersed liquid crystalline (PDLC) samples. Such materials[23] consist of uniformly aligned elongated cylindrical droplets of a liquid crystal in the S_A* phase that is embedded in a solid photoconducting poly(vinylcarbazole) matrix, which was prepared as described in section VI. In these PDLCs, the director of the S_A* phase is oriented in the direction of the long axes of the cylinders so that smectic layers are stacked along these same axes. Under the influence of a nonuniform illumination and an applied field, as is usual in photorefractive polymers, a space-charge field develops in the photoconducting polymer matrix. The total field (applied plus

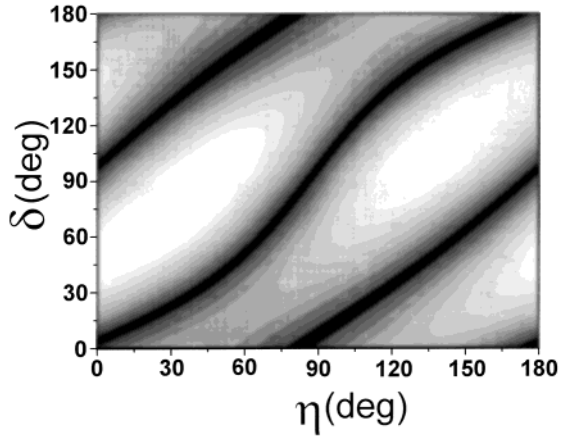

Figure 11. Gray-scale map of the absolute value of the refractive index modulation $|\Delta n|$ for a S_A* phase as a function of δ and η, calculated from eq 13. Lighter shades correspond to higher $|\Delta n|$ values. Between the edges of two adjacent areas, there is a difference in $|\Delta n|$ of 7.5×10^{-4}, and at the edge of the lightest area, $|\Delta n| = 8.25 \times 10^{-3}$. Data were obtained using the same values of the parameters as were used in Figure 10.

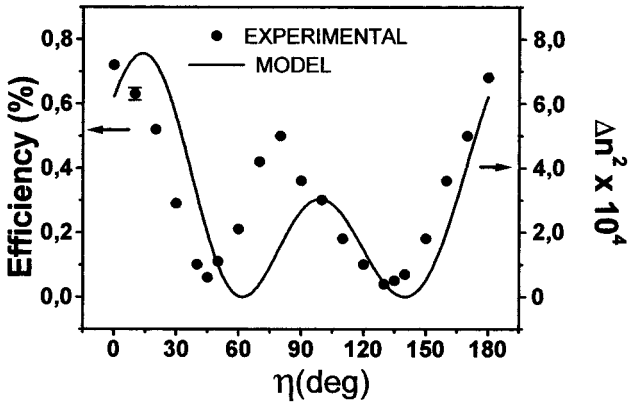

Figure 12. Experimental first-order diffraction efficiency as a function of light polarization for a sample consisting of cylindrical S_A* droplets dispersed in a photoconducting polymer. The weight composition of the sample was PVK/ECZ/TNFDM/E869 = 56:13:1:30, and data were obtained at $E_0 = 40$ V/μm by positioning the sample at $\delta = 54°$, $\theta = 31°$, and $\Omega = 1°$. The continuous line is the value of Δn^2 derived from eq 13 using the same parameters along with $k = 0.7$, $e_c = 0.19$ deg μm/V, $n_o = 1.5$, and $n_e = 1.6$. The values of Δn^2 inserted into the Figure have been multiplied by a common factor, as described in the text, to obtain the best fit to the experimental data for the efficiency.

space-charge) will induce a reorientation of the director of the S_A* phase within the droplets through the electroclinic effect, and a refractive index modulation will be established. In PDLCs, the dispersion of the mesophase domains effectively decouples the elastic energy from the director orientation in different droplets. In this case, it is then acceptable not to include the elastic terms in the calculation of the director reorientation, as we did in this article. On the other hand, surface effects present at the interfaces can be treated as effectively reducing the electroclinic coefficient when compared to the value measured in bulk samples.[24] For this reason, we measured e_c in our samples as described in section VI.

In Figure 12, we show the experimental first-order efficiency data from one of our chiral smectic A PDLC samples as a function of η for $\delta = 54°$, $\theta = 31°$, and $\Omega = 1°$ at a field of 40 V/μm together with the results obtained from eq 13 for $|\Delta n|^2$. In the determination of the index modulation from the model,

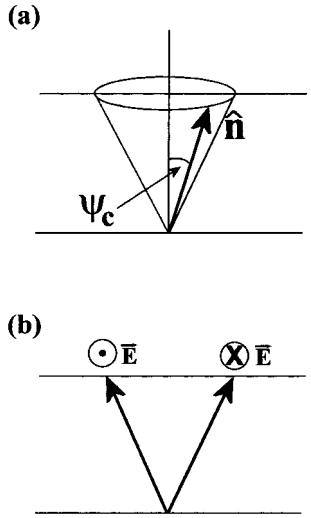

Figure 13. Illustration of (a) the director orientation within a S_C* layer and (b) the orientation induced by an electric field in the smectic layer.

the experimentally determined value of e_c and the value of $n_e - n_o$ of the liquid crystal provided by Merck were used. In fact, as a first-order approximation, the first-order efficiency and $|\Delta n|^2$ should be proportional.[1] In the proportionality constant we should also include the volume fraction of liquid crystalline droplets in our sample, which is unknown and hard to estimate, as well as the parameter k. For this reason, we chose to leave such proportionality constant as the only fitting parameter, which in other words means that the values of $|\Delta n|^2$ in Figure 12 have been multiplied by the proper constant to make the best fit of the experimental values of the efficiency. Given the single fitting parameter, the agreement with experiment is remarkable. The main discrepancy can be considered to be a shift of $\sim 20°$ in η between the model and the experiment, which could be explained by considering that our stretched PDLCs act as retarders and that the effective polarization within the sample is then modified. From ellipsometric measurements, we obtained a net phase retardation at the exit of the sample of $\sim 40°$, so that by considering an average polarization within the sample, which is 20° shifted with respect to the nominal polarization, the discrepancy could be accounted for.

IV. Extension to S_C* Phases

In this section, we will extend the model to S_C* phases. Such phases are ferroelectric, with a spontaneous polarization within the smectic layer and normal to the plane defined by the director and the layer normal. The director is spontaneously tilted with respect to the layer normal by an angle ψ_C, and in the absence of an orienting potential, any orientation of the director along a conical surface centered along the layer normal is possible, as illustrated in Figure 13a. A field within the layer will have the effect of reorienting the spontaneous polarization and thus the director, as described in Figure 13b. In the following discussion, we will assume that the component of the total field within the layers, $\vec{E}_{TL}$, is large enough for this reorientation to occur.

The calculation of the space-charge field components and of the director orientation and refractive index modulation carried out in sections II and III must be slightly modified to take into account the peculiarities of the S_C* phase. In particular, eqs 8, 13, and 14 are still valid, but eq 9 must be replaced by $\psi_C =$ constant and in eq 10 ψ_A must be replaced by ψ_C. The profile of the index modulation obtained in this case as a function of

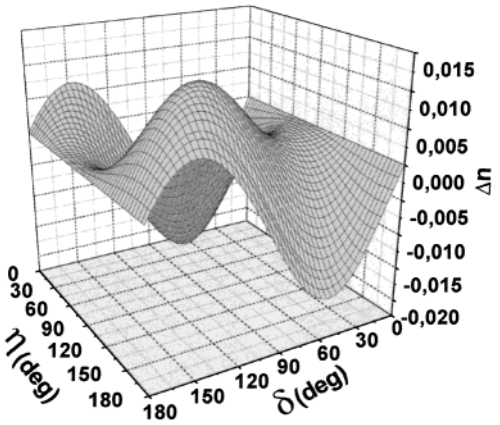

Figure 14. Refractive index modulation Δn in a S_C* phase as a function of δ and η, calculated from eq 13 for $k = 0.7$, $\psi_C = 19°$, $n_o = 1.5$, $n_e = 1.6$, $\theta = 31°$, and $\Omega = 1°$.

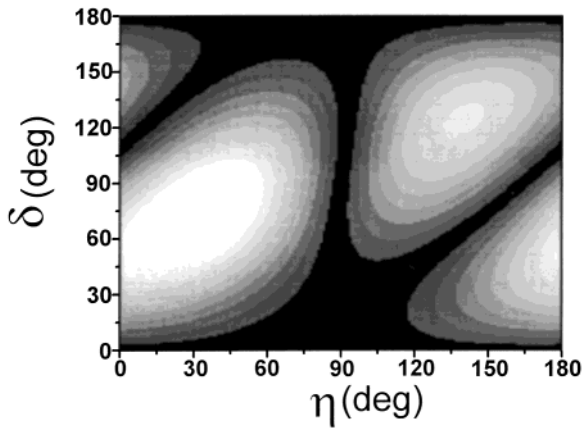

Figure 15. Gray-scale map of the absolute value of the refractive index modulation $|\Delta n|$ for a S_C* phase as a function of δ and η, calculated from eq 13. Lighter shades correspond to higher $|\Delta n|$ values. Between the edges of two adjacent areas there is a difference in $|\Delta n|$ of 1.33×10^{-3}, and at the edge of the lightest area, $|\Delta n| = 1.47 \times 10^{-2}$. Data were obtained using the same values of the parameters as were used in Figure 14.

δ and η is shown in Figure 14. The change of sign of Δn seems to be at least in qualitative agreement with the data reported in ref 16. In Figure 15, we instead illustrate the variation of $|\Delta n|$, obtained using the same parameters as are used in Figure 14, as a function of δ and η. When compared to the data of the S_A* of Figure 11, the index modulation for the S_C* shows two maxima more or less for the same values of δ and η as for those in the S_A* case. But now the two maxima are not of comparable amplitude because one is approximately 35% more intense than the other. In addition, for the S_C*, we obtain larger areas in the (δ, η) plane with negligible index modulation.

V. Conclusions

In this article, we developed a simple model to calculate the refractive index amplitude modulation in photorefractive chiral smectic A and C phases. In the model, we assume the simultaneous presence of an applied and a single harmonic space-charge electric field. The field-induced director reorientation in the smectics was assumed to be due to the electroclinic effect in the S_A* phases and to the coupling with spontaneous polarization in the S_C* phases. Several physical parameters were taken into account by the model, including liquid crystal birefringence, the electroclinic coefficient (for S_A*), the spontaneous tilt angle (for S_C*), and the relative amplitudes of the

applied and space-charge fields. In addition, sample orientation and light polarization were considered.

Position-dependent director orientations were first calculated, as a function of the parameters mentioned above, and from them, position-dependent refractive indices were obtained. The results show a large variation of index modulation with sample orientation and light polarization for both the S_A* and S_C* phases. Experimental determinations of first-order diffraction efficiencies as a function of polarization were conducted for samples consisting of S_A* cylindrical domains dispersed in a photoconducting polymer. Such data are in excellent agreement with the predictions of the model.

Finally, it should be mentioned that the approach presented here can be extended to other materials. In particular, this approach was used for nematics,[22] and it could certainly be extended to any material in which induced birefringence is important, even for purposes of tuning material properties.

VI. Experimental Section

The chiral smectic A liquid crystal mixture used for sample preparation was 869E from Merck with the following phase sequence: S_C* 15 °C, S_A* 69 °C, N* 82 °C I, where N* and I indicate the cholesteric and the isotropic phases, respectively. This liquid crystal was dispersed in a polymeric matrix where the main component was poly(vinylcarbazole) (PVK), but the matrix also contained ethylcarbazole (ECZ) as a plasticizer and 2,4,7-trinitro-9-fluorenylmalononitrile (TNFDM) as a photosensitizer. All these components were purchased from Aldrich and purified by recrystallization before use. The weight composition of samples was the following: PVK/ECZ/TNFDM/E869 = 56:13:1:30. To obtain the PDLC films, we dissolved all of the components in chloroform and induced phase separation by evaporation of the solvent at room temperature. The resulting films were about 200 μm thick and appeared opaque because of light scattering due to the random distribution of the director in the droplets. For our purposes, it was necessary to align the smectic layers in a uniform direction, and this was done by heating the film and, at the same time, by stretching it mechanically, thus deforming the droplets from a spherical to a cylindrical shape. It is known[23] that this process induces, after samples are cooled to room temperature, a uniform and permanent director orientation along the stretching direction (i.e., the smectic layers will, at the end, be stacked along the cylindrical symmetry axes of the droplets). Within each droplet, the director alignment is then like the alignment illustrated in Figure 1a. The thickness of the resulting films was thus reduced to 50−70 μm, and their scattering greatly decreased as a result of the uniform director orientation. The effectiveness of the orientation procedure was controlled by optical microscope observations with the sample placed between crossed polarizers.

The electroclinic coefficient of the liquid crystal within the elongated droplets was measured by monitoring light transmission when the sample was placed between crossed polarizers with the long axes of the droplets oriented with the incoming light polarization. When a field is applied, the induced tilt angle can be found by monitoring light transmission as a function of sample rotation. The electroclinic coefficient is then derived from the tilt angle. In our samples, we measured an electroclinic coefficient $e_c = 0.19$ deg μm/V.

We performed experiments of two beam coupling (2BC) by the overlapping of two coherent He−Ne beams (633 nm) on a circular area of the sample that was ∼0.8 mm in diameter and by monitoring the variation of transmitted light when an electric field was applied to the sample. The angle between the bisector of the beams and the sample normal was 60°, and the intensity of both beams was 3 mW. By changing the angle between the two incident beams, we could obtain several values of the grating spacing Λ. For the experiments reported in this article, we worked with $\Lambda = 10$ μm. Given this grating spacing, we worked with a value of the parameter $Q = 2\pi\lambda d/n\Lambda^2 \approx 1$ (i.e., we operated in the Raman−Nath diffraction regime and observed several diffraction orders). We obtained the first-order efficiency by dividing the intensity of the first-order diffraction by the intensity of the zeroth-order beam in the absence of the grating. To carry out the measurement, we illuminated the sample with both incident beams, turned on the electric field, and waited at least 3 min before measuring the intensity of the first-order diffraction beam.

Acknowledgment. This research was supported by research grants from the Italian Ministero dell'Università e della Ricerca Scientifica e Tecnologica (MURST).

References and Notes

(1) Yeh, P. *Introduction to Photorefractive Nonlinear Optics*; Wiley & Sons: New York, 1993.
(2) Solymar, L.; Webb, D. J.; Grunnet-Jepsen, A. *The Physics and Applications of Photorefractive Materials*; Clarendon: Oxford, U.K., 1996.
(3) Ashkin, A.; Boyd, G. D.; Dziedzic, J. M.; Smith, R. G.; Ballman, A. A.; Levinstein, J. J.; Nassau, K. *Appl. Phys. Lett.* **1966**, *9*, 72.
(4) Sutter, K.; Günter, P. *J. Opt. Soc. Am. B* **1990**, *7*, 2274.
(5) Ducharme, S.; Scott, J. C.; Twieg, R. J.; Moerner, W. E. *Phys. Rev. Lett.* **1991**, *66*, 1846.
(6) Meerholz, K.; Volodin, B. L.; Sandalphon; Kippelen, B.; Peyghambarian, N. *Nature (London)* **1994**, *371*, 497.
(7) Moerner, W. E.; Grunnet-Jepsen, A.; Thompson, C. L. *Annu. Rev. Mater. Sci.* **1997**, *27*, 585.
(8) Bässler, H. *Phys. Status Solidi B* **1993**, *175*, 15.
(9) Moerner, W. E.; Silence, S. M.; Hache, F.; Bjorklund, G. C. *J. Opt. Soc. Am. B* **1994**, *11*, 320.
(10) Rudenko, E. V.; Sukhov, A. V. *JETP Lett.* **1994**, *59*, 142.
(11) Khoo, I. C.; Li, H.; Liang, Y. *Opt. Lett.* **1994**, *19*, 1723.
(12) Wiederrecht, G. P.; Yoon, B. A.; Wasielewski, M. R.; *Science (Washington, D.C.)* **1995**, *270*, 1794.
(13) Wiederrecht, G. P.; Niemczyk, M. P.; Svec, W. A.; Wasielewski, M. R. *Chem. Mater.* **1999**, *11*, 1409.
(14) Ono, H.; Kawatsuki, N. *Opt. Lett.* **1997**, *22*, 1144.
(15) Golemme, A.; Volodin, B. L.; Kippelen, B.; Peyghambarian, N. *Opt. Lett.* **1997**, *22*, 1226.
(16) Wiederrecht, G. P.; Yoon, B. A.; Wasielewski, M. R. *Adv. Mater. (Weinheim, Ger.)* **2000**, *12*, 1533.
(17) Termine, R.; De Simone, B. C.; Golemme, A. *Appl. Phys. Lett.* **2001**, *78*, 688.
(18) Termine, R.; Golemme, A. *Opt. Lett.* **2001**, *26*, 1001.
(19) Muševič, I.; Blinc, R.; Žekš, B. *The Physics of Ferroelectric and Antiferroelectric Liquid Crystals*; World Scientific: Singapore, 2000.
(20) Lagerwall, S. T. *Ferroelectric and Antiferroelectric Liquid Crystals*; Wiley-VCH: Weinheim, Germany, 1999.
(21) Lagerwall, S. T.; Matuszczyk, M.; Rodhe, P.; Ödman, L. In *The Optics of Thermotropic Liquid Crystals*; Elston, S., Sambles, R., Eds.; Taylor and Francis: London, 1998; p 155.
(22) Golemme, A.; Kippelen, B.; Peyghambarian, N. *Chem. Phys. Lett.* **2000**, *319*, 655.
(23) Aloe, R.; Nicotera, I.; Golemme, A. *Appl. Phys. Lett.* **1999**, *75*, 343.
(24) Kitzerow, H.-S. In *Liquid Crystals in Complex Geometries*; Crawford, G. P., Žumer, S., Eds.; Taylor and Francis: London, 1996; p 187.